Characterization and Modeling of Metallocene-Based Branch−Block Copolymers

Armenag H. Dekmezian,*,† Joao B. P. Soares,‡ Peijun Jiang,† Cesar A. Garcia-Franco,† Weiqing Weng,† Hitesh Fruitwala,† Thomas Sun,† and Deborah M. Sarzotti‡

Baytown Polymers Center, ExxonMobil Chemical Company, 5200 Bayway Drive, Baytown, Texas 77522, and Institute for Polymer Research, Department of Chemical Engineering, University of Waterloo, Waterloo, Ontario, Canada N2L 3G1

Received June 14, 2002; Revised Manuscript Received August 22, 2002

ABSTRACT: The nature of polyolefin branch−block copolymers produced using mixed-metallocene catalysts has been further characterized in an attempt to relate polymer microstructure to properties. These copolymers were synthesized by incorporating vinyl-terminated, crystallizable macromonomers into amorphous backbones. It was shown that polymer properties depended strongly on the fine details of the polymerization procedure (sequential or ex-situ vs simultaneous or in-situ). Here we present rheological, chromatographic, and thermal data along with polymerization kinetic model simulations to interpret the observed property differences between ex-situ and in-situ produced polymers.

Introduction

The tailoring of polyolefin molecular profile through nanodesign of single-site catalyst systems has been the subject of many studies.[1] By proper selection of catalyst and reactor process variables, one can control the various distributions that describe molecular size, composition, and long-chain branching (LCB), all of which affect polymer properties.[2,3] The knowledge gained to date on how single-site catalyst systems performing in different environments is a stepping stone toward understanding more complex systems, such as mixed-catalyst or mixed-activator systems.[2−10] Besides the polymeric species generated by the individual catalysts, the polymers produced by a mixed-catalyst system may contain cross products. The cross products are formed when one catalyst produces reactive macromonomers that are utilized by the other catalyst during chain propagation, thus generating long-chain branch architectures of diverse compositions.[2,8] Such branched species, even when present at minute concentrations, can significantly alter the polymer property profile.[11] Our ability to control the type and population of these cross products will depend on developing reactor-engineering models and advanced characterization capabilities, in addition to our knowledge of catalyst systems. This paper describes the characterization and modeling of branch−block copolymers made using a pair of metallocene catalysts. The paper is aimed at relating polymerization process conditions to polymer compositions and microstructures that may be further related to the polymer property profiles.[3]

The polymers discussed here were made in a solution reactor using a mixed-metallocene catalyst system and a monomer feed consisting of ethylene and 1-butene. One of the catalysts ("linear catalyst") is chosen because it has low comonomer incorporating capability and produces linear crystalline chains and macromonomers with size distribution having Flory most probable distribution; the particular catalyst used here was bis(cyclopentadienyl)zirconium dichloride activated with methylalumoxane. The other catalyst ("LCB catalyst") is chosen to have high reactivity ratios toward comonomer and macromonomer incorporation. The LCB catalyst, which in this case was dimethylsiladiyl(tetramethylcyclopentadienyl) (cyclododecamido)titanium dichloride activated with methylalumoxane, produces chains with amorphous backbones having branches of crystalline or amorphous macromonomers, as illustrated in Figure 1.

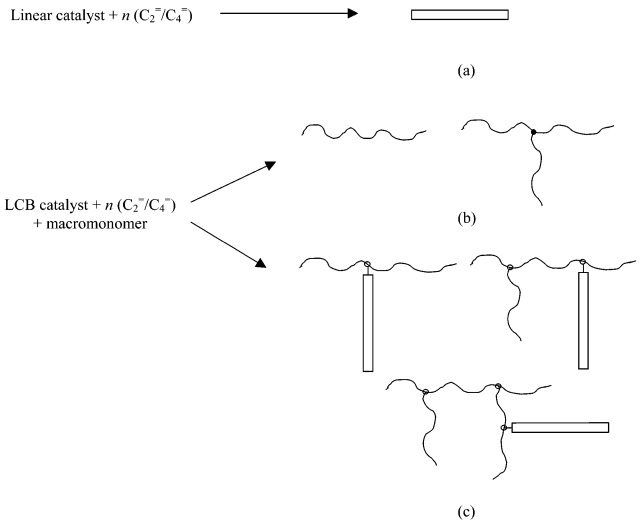

Figure 1. Mechanism of chain formation with dual metallocene systems. The linear catalyst has low reactivity ratio toward α-olefins and makes only (a) linear crystalline chains and macromonomers. The LCB catalyst has high reactivity toward α-olefins and makes (b) linear and branched amorphous chains and (c) semicrystalline branch−block chains. Chains containing more branches made by the LCB catalyst are possible but not shown here for brevity.

The linear catalyst may be selected from the bis(cyclopentadienyl) catalyst families that typically have low comonomer incorporating capability. The LCB catalyst could be chosen from a similar family or could

† ExxonMobil Chemical Company.
‡ University of Waterloo.

10.1021/ma0209343 CCC: $22.00
Published on Web 11/02/2002

be from the family of monocyclopentadienyl catalysts that have high comonomer incorporating capability. The selection of the appropriate pair is critical in controlling the types of polymer species produced.

As for the macromonomer, the characteristics of the catalyst producing it and the process conditions strictly govern its crystalline nature as well as its size distribution. The cross products may range in architecture from 3-arm stars to combs to hyperbranched topologies.[11,12] The distribution of species may be modeled using statistical techniques. The cross products may be homogeneous or heterogeneous in composition, as indicated in Figure 1, depending on the compositional similarity between the backbone and the long chains.

The definition of long chain is relative to the intended effect on properties. If the macromonomer is polyethylene and one is interested in studying how its crystallization characteristics affect mechanical properties, then its length must be at least eight carbons long.[13] If the macromonomer is intended for altering viscoelastic characteristics, then it must have size dimensions larger than the entanglement molecular weight (M_e).[14]

How chain topological variations affect properties is an evolving field, and attempts are underway to classify and model these complex variations.[11,12] Our focus here will be on the analytical characterization and the kinetic modeling of polyolefin branch−block copolymers, in which the backbone and the LCB have different composition.

An example of such a heterogeneous composition was described in an earlier paper.[3] Some of these copolymers, which are thought to consist of amorphous backbones from which crystallizable long chains emanate, were shown to display thermoplastic elastomer properties. The polymer properties were shown to depend on the catalyst pair selected and the details of the polymerization scheme. A polymer in which the macromonomer was prepolymerized and then introduced into the reactor gave distinctly different property profile compared to one where the macromonomer and the backbone were cogenerated in the same reactor. The two polymers had different microphase separation patterns, shear sensitivity, tensile, and elastic properties as compared to those of a highly elastic hydrogenated styrene−isoprene-styrene triblock copolymer.

Since the reactor product was a complex mixture of species, model studies were undertaken to assess the nature of the LCB distribution. The model studies showed that the LCB species were concentrated in the high molecular weight tail, becoming significant past the number-average molecular weight region and progressively getting more branched with increasing molecular weight. Some of the high molecular weight components had over 10−60 LCB/chain, depending on the catalyst and process used. The nature of the high molecular weight long chain branched tail was thought to underline the observed properties, but not enough evidence was presented at that time. We decided to investigate the nature of the cross product in more detail, as shown below.

In this work we provide additional gel permeation chromatographic (GPC), thermal, rheological, and reactor kinetic modeling results to differentiate and characterize the molecular architectures of two branch−block copolymers that have different property profiles. Also, reactor kinetic simulations were made to model the generation of the various reactor products as a function of polymerization condition, namely when macromonomers are produced ex-situ or in-situ.

Mathematical Model Development

The structural evolution of branch−block compositions can be described using polymerization reaction kinetics. It will be assumed that there is no interaction between the mixed catalysts: the linear catalyst produces linear polymer with saturated and unsaturated chain ends (macromonomers), while the LCB catalyst produces linear polymer chains as well as incorporate the macromonomers to form branch−block structures. The linear catalyst affects the system only through the production of unsaturated macromonomers and linear dead chains. Under this assumption, the basic kinetic steps derived from each individual catalyst can describe the polymerization reactions in the mixed-catalyst system. The connection between the two catalysts is described through the macromonomer incorporation step.

A polymerization kinetic model was developed to trace the evolution of linear and branched structures during polymerization in a semibatch reactor for both in-situ and ex-situ operations. A statistical model was also used to describe the molecular weight distribution of branched species. The possible branched structures are illustrated in Figure 1 and include poly(ethylene-*co*-1-butene) grafted onto poly(ethylene-*co*-1-butene) (EB-*g*-EB) and polyethylene grafted onto poly(ethylene-*co*-1-butene) (EB-*g*-PE), as well as higher levels of grafting derivatives such as EB-*g*-(EB-*g*-PE). These fine details are not differentiated in the present mathematical model due to lower probability of formation of chains with higher levels of grafting.

Population Balance Model. The mathematical model developed below monitors only the molar fraction of linear chains, homogeneous branched chains (backbone and LCB of the same type), and heterogeneous branched chains (at least one LCB differs from the backbone). Molecular weight is not described in this model. (A more detailed version of this model, including molecular weight distribution predictions, is beyond the objectives of the present investigation and will be published elsewhere.[15]) The model applies to semibatch polymerization under constant ethylene pressure, which were the conditions used for the synthesis of the polymer samples studied in this investigation.

Polymerization Mechanism for ex-Situ LCB Formation. In this case, polyethylene (PE) macromonomer made with the linear catalyst in a separate polymerization run is added to the reactor containing the LCB catalyst. At any time during polymerization with the LCB catalyst a complex mixture of chains will be present in the reactor:[1] PE linear chains added to the reactor and linear poly(ethylene-*co*-1-butene) (EB) chains made by the LCB catalyst;[2] homogeneous branched chains of the type EB-*g*-EB, and[3] heterogeneous branched chains of the type EB-*g*-PE. Several higher levels of grafting will also occur, e.g., EB-*g*-(PE-*g*-PE), EB-*g*-(PE-*g*-EB), EB-*g*-(EB-*g*-PE), but as mentioned above, the present model will not describe these fine microstructural details.

The mechanism for branch formation used for model development is detailed in Table 1. For simplicity, it is assumed that all dead chains contain terminal vinyl unsaturations. Catalyst deactivation is also neglected. All branch-formation reactions are assumed to have the

Table 1. Mechanism for ex-Situ and in-Situ Polymerizations Used with the Population Balance Models[a]

ex-situ	in-situ catalyst 1	in-situ catalyst 2[b]	kinetic constants
	Branch Formation Reactions		
$P + m \rightarrow P_m$	$P_1 + D_1 \rightarrow P_{b1}$	$P_2 + D_2 \rightarrow P_{b2}$	k_{D1}, k_{D2}
$P + D \rightarrow P_b$	$P_1 + D_2 \rightarrow P_{m1}$	$P_2 + D_1 \rightarrow P_{m2}$	k_{D1}, k_{D2}
$P + D_b \rightarrow P_b$	$P_1 + D_{b1} \rightarrow P_{b,1}$	$P_2 + D_{b2} \rightarrow P_{b,2}$	k_{D1}, k_{D2}
$P + D_m \rightarrow P_m$	$P_1 + D_{b2} \rightarrow P_{m,1}$	$P_2 + D_{b1} \rightarrow P_{m,2}$	k_{D1}, k_{D2}
$P_b + m \rightarrow P_m$	$P_1 + D_m \rightarrow P_{m,1}$	$P_2 + D_m \rightarrow P_{m,2}$	k_{D1}, k_{D2}
$P_b + D_b \rightarrow P_b$	$P_{b1} + D_1 \rightarrow P_{b1}$	$P_{b2} + D_2 \rightarrow P_{b2}$	k_{D1}, k_{D2}
$P_b + D_m \rightarrow P_m$	$P_{b1} + D_2 \rightarrow P_{m1}$	$P_{b2} + D_1 \rightarrow P_{m2}$	k_{D1}, k_{D2}
	$P_{b1} + D_{b1} \rightarrow P_{b1}$	$P_{b2} + D_{b2} \rightarrow P_{b2}$	k_{D1}, k_{D2}
	$P_{b1} + D_{b2} \rightarrow P_{m1}$	$P_{b2} + D_{b1} \rightarrow P_{m2}$	k_{D1}, k_{D2}
	$P_{b1} + D_m \rightarrow P_{m1}$	$P_{b2} + D_m \rightarrow P_{m2}$	k_{D1}, k_{D2}
	Termination Reactions		
$P \rightarrow D + C^*$	$P_1 \rightarrow D_1 + C_1^*$	$P_2 \rightarrow D_2 + C_2^*$	$k_{\beta 1}$, $k_{\beta 2}$
$P_b \rightarrow D_b + C^*$	$P_{b1} \rightarrow D_{b1} + C_1^*$	$P_{b2} \rightarrow D_{b2} + C_2^*$	$k_{\beta 1}$, $k_{\beta 2}$
$P_m \rightarrow D_m + C^*$	$P_{m1} \rightarrow D_m + C_1^*$	$P_{m2} \rightarrow D_m + C_2^*$	$k_{\beta 1}$, $k_{\beta 2}$

[a] Definitions: m = macromer, P = living linear chain, D = dead linear chain, P_b = living homogeneous-branched chain, D_b = dead homogeneous-branched chain, P_m = living heterogeneous-branched chain, D_m = dead heterogeneous-branched chain. For in-situ polymerization, subscripts 1 and 2 indicate catalyst type. [b] For the sake of completeness, it is considered that both catalyst 1 and 2 are allowed to form branches. For the simulations of the particular system considered in this investigation, the rate constant of branch formation for the linear catalyst, k_{D2}, is set to zero.

same reaction rate constant (k_D), and all transfer reactions are considered to be by β-hydride elimination, also with the same kinetic rate constant (k_β). The model can be easily extended to include more detailed polymerization kinetic steps, but the simplified version presented herein leads to simpler equations that are ideal to achieve the main objective of this investigation, i.e., to compare the microstructures of polymers made by in-situ and ex-situ polymerizations.

Model equations for the molar fractions of chain populations were obtained by developing population balances for living and dead species and making the pseudo-steady-state approximation for the living chains. Table 2 shows the resulting differential−algebraic system of equations needed to model this process.

Polymerization Mechanism for in-Situ LCB Formation. The mechanism for in-situ polymerization is also presented in Table 1. The general model assumes that both catalysts can form LCB chains. For our particular simulations, only the LCB catalyst forms LCB, while the linear catalyst makes only linear chains. This is easily achieved by setting the rate constant for branch formation for catalyst 2, k_{D2}, to zero. Similarly, model equations are obtained by population balances, making the pseudo-steady-state approximation for the living polymer chains, as shown in Table 2. Note that for the case when $k_{D2} = 0$, $x_{b2} = y_{b2} = y_{m2} = 0$; i.e., catalyst 2 (linear catalyst) does not produce branched species of any type, as required for our experiments.

Statistical Model. In this approach, it is assumed that EB-*g*-PE structures are the only branched species formed during the polymerization; these structures are formed through the random grafting of preformed PE macromonomers onto EB backbones. The probability for a backbone with r monomer units and b branch points can be described by a binomial distribution.[16] In most cases, the number of branch points is much smaller than the number of monomer units on the backbone. Thus,

Table 2. Population Balance Equations for in-Situ and ex-Situ Models[a]

description	in-situ	ex-situ
molar fraction of dead linear chains	$\frac{dx}{dt} = \frac{k_\beta Y}{Q}(y - x)$	$\frac{dx_1}{dt} = \frac{Y}{Q}[k_{\beta_1}(y_1 + \mu_1 x_1) - k_{\beta_2}\mu_2 x_1]$ $\frac{dx_2}{dt} = \frac{Y}{Q}[k_{\beta_2}(y_2 + \mu_2 x_2) - k_{\beta_1}\mu_1 x_2]$
molar fraction of dead homogeneous branched chains	$\frac{dx_b}{dt} = \frac{k_\beta Y}{Q}(y_b - x_b)$	$\frac{dx_{b1}}{dt} = \frac{Y}{Q}[k_{\beta 1}(y_{b1} + \mu_1 x_{b1}) - k_{\beta 2}\mu_2 x_{b1}]$ $\frac{dx_{b2}}{dt} = \frac{Y}{Q}[k_{\beta 2}(y_{b2} + \mu_2 x_{b2}) - k_{\beta 1}\mu_1 x_{b2}]$
molar fraction of dead heterogeneous branched chains	$\frac{dx_m}{dt} = \frac{k_\beta Y}{Q}(y_m - x_m)$	$x_m = 1 - x_1 - x_{b1} - x_2 - x_{b2}$
molar fraction of macromonomer added to the reactor	$x_{mm} = 1 - x - x_b - x_m$	
molar fraction of living linear chains	$y = \frac{k_\beta}{k_D Q + k_\beta}$	$y_1 = \frac{k_{\beta 1}\mu_1}{k_{D1}Q + k_{\beta 1}}$ $y_2 = \frac{k_{\beta 2}\mu_2}{k_{D2}Q + k_{\beta 2}}$
molar fraction of homogeneous living chains	$y_b = \frac{k_D Q y(x + x_b)}{k_D Q(x_m + x_{mm}) + k_\beta}$	$y_{b1} = \frac{k_{D1}Q y_1(x_1 + x_{b1})}{k_{D1}Q(x_2 + x_{b2} + x_m) - k_{\beta 1}}$ $y_{b2} = \frac{k_{D2}Q y_2(x_2 + x_{b2})}{k_{D2}Q(x_1 + x_{b1} + x_m) - k_{\beta 2}}$
molar fraction of heterogeneous living chains	$y_m = 1 - y - y_b$	$y_{m1} = \frac{k_{D1}Q(y_1 + y_{b1})(x_2 + x_{b2} + x_m)}{k_{\beta 1}}$ $y_{m2} = 1 - y_1 - y_{b1} - y_{m1} - y_2 - y_{b2}$
total concentration of dead chains in the reactor	$Q = \frac{k_\beta}{k_D}(1 - e^{-k_D Y t}) + m_0 e^{-k_D Y t}$	$Q = \frac{k_{\beta 1}\mu_1 + k_{\beta 2}\mu_2}{k_{D1}\mu_1 + k_{D2}\mu_2}\{1 - \exp[-(k_{D1}\mu_1 + k_{D2}\mu_2)Yt]\}$

[a] Y is the total concentration of catalyst. For the ex-situ model, m_0 is the initial concentration of macromonomer. For the in-situ model, the subscripts 1 and 2 indicate catalyst type, and μ_1 and μ_2 are the molar fractions of catalyst 1 and 2, respectively.

the binomial distribution can be approximated by a Poisson distribution, i.e.,

$$\frac{(\lambda r)^b}{b!}\exp(-\lambda r) \tag{1}$$

where λ is the probability of macromonomer insertion or branch density (number of branch points per backbone monomer). The molar concentration of chains with r units on the backbone, b branch points and a total of s monomer units on all the branches can be expressed as

$$n_c(r,s,b) = n_B(r)\frac{(\lambda r)^b}{b!}\exp(-\lambda r)\zeta_b(s) \tag{2}$$

where $n_B(r)$ is the number distribution of molecular weight for the backbone. $\zeta_b(s)$ is the mole fraction of branches with a total chain length of s monomeric units; this can be obtained from the molecular weight distribution of branches.[17] Assuming that the molecular weight distribution of the branches follows the Schulz−Zimm distribution,

$$n(s) = \frac{1}{(k-1)!}\frac{k}{M_{ns}}\left(\frac{ks}{M_{ns}}\right)^{k-1}\exp\left(-\frac{ks}{M_{ns}}\right) \tag{3}$$

Gu et al.[17] derived the following equation for the number distribution of comb-branched copolymers:

$$n_c(r,s,b) = n_B(r)\frac{(\lambda r)^b\exp(-\lambda r)}{b!(kb-1)!}\frac{k}{M_{ns}}\left(\frac{ks}{M_{ns}}\right)^{kb-1}\exp\left(-\frac{ks}{M_{ns}}\right) \tag{4}$$

where M_{ns} is the number-average molecular weight of branches; k is related to the polydispersity of the branches and is defined as:

$$k = \frac{M_{ns}}{M_{ws}-M_{ns}} \quad \text{or} \quad \frac{M_{ws}}{M_{ns}} = \frac{k+1}{k} \tag{5}$$

The mole fraction of linear backbone is given by:

$$n_{c,0}(r) = n_B(r)(1-\lambda)^r = n_B(r)\exp(-\lambda r) \tag{6}$$

The population distribution of branched species can be described as a function of the number of branches using eq 4. The parameters required for a model calculation involve the number of branches, molecular weight distribution, and branching density. The molecular weight distribution can be obtained using GPC techniques while the number of branches can be obtained using FTIR or other techniques that may involve labeling of various types. The branch density can be calculated using reaction kinetics involving macromonomer incorporation. Comb structures are formed when macromonomers are added through insertion mechanism into backbone. It is assumed that all reactive double bonds have the same copolymerization reactivity regardless of chain length. The reaction pathways can be described using the reaction steps outlined in the Appendix. Branch formation depends on the competition between monomers and macromonomers; the branching density can be written as

$$\lambda = \frac{\text{macromonomer incorporation rate}}{\text{propagation rate} + \text{macromonomer incorporation rate}} \tag{7}$$

Experimental Section

Materials/Synthesis. The two samples of interest are labeled ex-situ and in-situ. Their synthesis conditions and select properties, extracted from an earlier paper,[3] are summarized in Table 3. The ex-situ product was made sequentially whereby the macromonomer was first made and then allowed to be consumed in the second, assembly stage. In the in-situ case, the macromonomers and the backbone were formed simultaneously.

As described elsewhere,[3] all catalyst preparations were performed in an inert atmosphere with <1.5 ppm of H_2O content. Metallocene catalyst precursors were activated with either methylalumoxane (MAO, 10% in toluene, from Albemarle Inc.) or dimethylanilinium tetrakis(perfluorophenyl)borate (Boulder Scientific Co.). The catalyst was added to a stainless steel tube by pipet and transferred to the reactor.

Macromonomer synthesis was conducted in a 1 L Zipperclave reactor equipped with a water jacket for temperature control. High-purity (>99.5%) solvent (toluene or hexane, 600 mL) and comonomer (butene) were introduced into the reactor, the temperature of which was set at 90 °C, and the system was allowed to reach equilibrium. The ethylene pressure regulator was set to 20 psi above the reactor pressure, and ethylene was added to the reactor until a steady-state condition was achieved, as measured by zero ethylene uptake. Catalyst was injected using a catalyst tube, and the ethylene supply manifold was immediately opened to the reactor in order to maintain a constant reactor pressure as ethylene was consumed. The reaction medium was mixed using a flat-paddle stirrer rotating at 750 rpm. Injecting methanol after 15−30 min terminated the reaction. The product was poured into excess isopropyl alcohol to precipitate the polymer that was then evaporated to dryness.

The ex-situ polymerization was conducted in a 2 L autoclave reactor. In one experiment, the reactor was charged with toluene (300 mL), macromonomer (5−30 g), and triisobutylaluminum (0.5 mL of 1 M solution in toluene), followed by an appropriate amount of monomer and comonomer. The reactor was heated to the desired temperature and equilibrated for 5 min, and then the catalyst and the activator (in 3 mL of toluene) were injected. After 15−20 min, the reactor was cooled to 25 °C and vented. The product was poured into excess isopropyl alcohol to precipitate the polymer, which was then dried in air overnight.

To synthesize in-situ branch−block copolymers, the reactor was purged with nitrogen and pressure tested using ethylene. Solvent (toluene, 600 mL) and comonomer (butene, 20 mL) were added to the reactor. The reactor temperature controller was set to 90 °C, and the system was allowed to reach equilibrium. The ethylene pressure regulator was next set to 100 psig, and ethylene was added to the system until a steady state was achieved, as measured by zero ethylene uptake. The mixed-catalyst (Cp_2ZrCl_2 and $(C_5Me_4SiMe_2NC_{12}H_{23})TiCl_2$) activated with 10% methylalumoxane (MAO) solution in toluene was injected. The 100 psig ethylene supply manifold was immediately opened to the reactor in order to maintain a constant reactor pressure as ethylene was consumed by reaction. Injecting methanol after 7 min terminated the reaction. The product was poured into excess isopropyl alcohol and evaporated to dryness.

Gel Permeation Chromatography. The gel permeation chromatography data were taken on a high-temperature GPC equipped with an online LALLS detector and viscometer. The details of the detector calibrations have been described else-

Table 3. Characterization of Branch−Block Copolymers

		GPC-DRI/viscometer/LALLS						tensile properties[d]		
sample	polymerization[a]	M_n ($\times 10^3$)	M_w ($\times 10^3$)	M_z ($\times 10^3$)	M_w/M_n	M_z/M_w	$g'_{(avg)}$	tensile strength (psi)	elongation at break (%)	recovery (%)
ex-situ	sequential[b]	87	281	775	4.4	2.7	0.961	2401	905	76
in-situ	simultaneous[c]	225	466	785	2.5	1.7	0.996	3054	669	87

[a] Polymerization temperature = 90 °C. Catalysts: bis(pentadienyl)zirconium dichloride activated with methylalumoxane (MAO, 10% in toluene) and dimethylsiladiyl (tetramethylcyclopentadienyl) (cyclododecamido)titanium dichloride activated with methylalumoxane (MAO, 10% in toluene). [b] Ex-situ means C_2^{2-}/C_4^{2-} macromonomer was first synthesized and then copolymerized with C_2^{2-}/C_4^{2-}. [c] In-situ synthesis of macromonomer and backbone using mixed metallocene catalyst. [d] Standard tensile testing was performed on an Instron 4505 instrument at room temperature using ASTM Method D1708. Elastic recovery was measured at 150% stain.

where;[19] attached below are brief descriptions of the components. A Waters 150C high-temperature GPC with three Polymer Laboratories PLgel 10 mm Mixed-B columns, a nominal flow rate 0.5 cm^3/min, and a nominal injection volume 300 μL is common to both detector configurations. The various transfer lines, columns, and differential refractometer (the DRI detector, used mainly to determine eluting solution concentrations) are contained in an oven maintained at 135 °C.

The LALLS detector is the model 2040 dual-angle light scattering photometer (Precision Detector Inc.). Its flow cell, located in the SEC oven, uses a 690 nm diode laser light source and collects scattered light at two angles, 15° and 90°. Only the 15° output was used in these experiments. Its signal is sent to a data acquisition board (National Instruments) that accumulates readings at a rate of 16 per second. The lowest four readings are averaged, and then a proportional signal is sent to the SEC-LALLS-VIS computer. The LALLS detector is positioned after the SEC columns, but before the viscometer.

The viscometer is a high-temperature model 150R (Viscotek Corp.). It consists of four capillaries arranged in a Wheatstone bridge configuration with two pressure transducers. One transducer measures the total pressure drop across the detector, and the other, positioned between the two sides of the bridge, measures a differential pressure. The specific viscosity for the solution flowing through the viscometer is calculated from their outputs. The viscometer is inside the SEC oven, positioned after the LALLS detector but before the DRI detector.

Rheology. The linear viscoelastic properties were obtained with an Advanced Rheometrics Expansion system (ARES) rheometer using 25 mm parallel plate geometry. Experimental specimens were stabilized and compression-molded at 190. Care was exercised to ensure linear viscoelastic response. Isothermal frequency sweeps were performed at various temperatures over $10^{-2} < \omega < 390$ rad/s.

Crystaf. Crystallization analysis fractionation (Crystaf) uses a unique approach to monitor the solution crystallization of polymers. The crystallization is carried out in 60 mL stirred vessels where dissolution and filtration take place automatically.[20] The analysis is carried out by monitoring the polymer solution concentration during crystallization as the temperature is reduced. The dual wavelength infrared detector together with a heated follow-through microcell is used to measure the concentration. Samples are prepared by dissolving 30 mg of polymer sample in 30 mL of 1,2,4-trichlorobenzene at 160 °C for 60 min and then rapidly cooled to 100 °C at a rate of 25 °C/min. This is followed by a slow cooling step in which the polymer solution is cooled at a rate of 0.2 °C/min between 100 and 30 °C. The initial polymer concentration is assigned a 100% value, and a pure solvent is defined as 0%. A derivative of the concentration vs temperature curve provides a pictorial representation of the branching distribution.

Results and Discussion

Molecular Weight Distribution and Long-Chain Branching. Table 3 summarized the GPC-DRI/viscometer/LALLS data on the two polymers. Since the two polymers were run under different batch reactor conditions (see Experimental Section), it is not surprising that their molecular weights are different (because of such differences as impurities and chain-transfer mechanisms). However, the molecular weight distribution (MWD) and its moments tell us a story that is consistent with the kinetic model. The multidetector GPC data show that the ex-situ product has much broader molecular weight distribution ($M_w/M_n = 3.2$) compared to the in-situ product ($M_w/M_n = 2.1$). That the branching density is higher in the ex-situ product, particularly at the high MW ends, is supported by the higher M_z/M_w value for ex-situ ($M_z/M_w = 2.7$) compared to the in-situ ($M_z/M_w = 1.7$).

The branching index, g', shows how the branching increases with increasing molecular weight, as evidenced by the progressively lower value of the g' factor (a g' of 1.0 indicates linear polymer chain). This trend is further supported by the intrinsic viscosity data. The fact that the polymer solution viscosity is lower than that of the linear reference, and that it gets progressively lower with increasing molecular weight, indicates the increasing level of long-chain branching as a function of molecular weight.

Even though LALLS and intrinsic viscometer data give clear evidence of the presence of long chain-branched species, they are not discriminating enough to allow fingerprinting the small but significant differences between the two samples. Rheological techniques were therefore used to map these fine differences.

Rheology. Some LCB structures exhibit a power law relaxation behavior over a finite frequency range.[21,22] As a consequence, G' and G'' scale with frequency as ω^n and tan δ becomes frequency independent over that finite frequency range. Figure 2 shows the complex moduli as a function of frequency at 210 °C for ex-situ and in-situ samples. It can be observed that the dynamic moduli of both samples is nearly parallel in the low-frequency region, and consequently the tangent of the phase angle becomes independent (or nearly independent) of frequency which is confirmed by Figure 3, indicating the presence of LCB. The tan δ of a linear (hydrogenated polybutadiene) polyethylene is included in this figure as a reference. Furthermore, the tan δ of the ex-situ sample is lower than that of the in-situ at low frequencies. This is a good indication that the ex-situ sample has more LCB than the in-situ material.[21−23] This is not surprising since, as will be discussed in the modeling section, the macromonomer is abundantly available during ex-situ polymerization, while in the in-situ case the macromonomers have to be produced as the polymerization progresses before they can be used to form branched chains. This section is meant to establish the presence of long-chain branching in these materials rather than more detailed information on the branched structures.

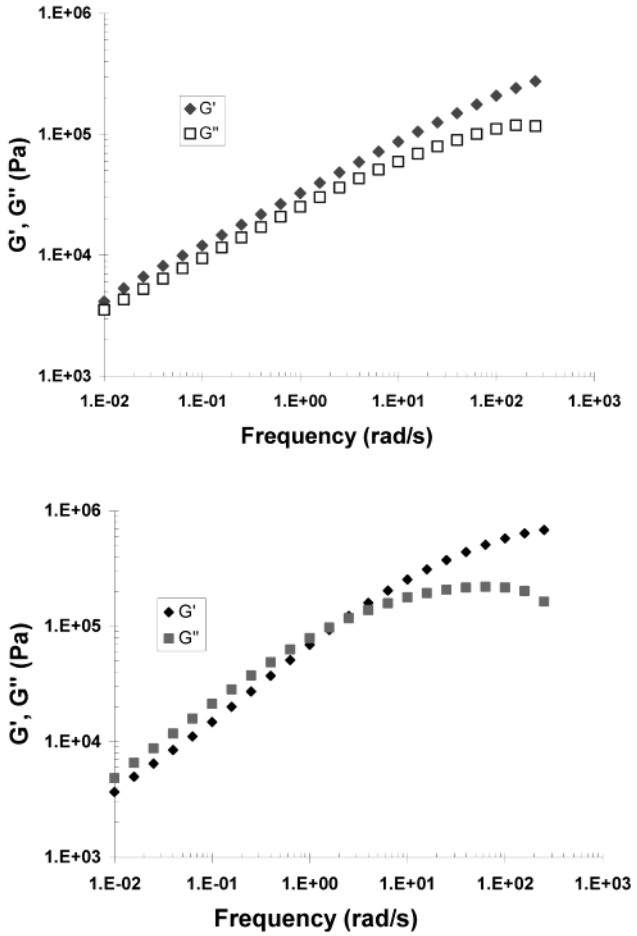

Figure 2. *G′* and *G″* of ex-situ (top) and in-situ (bottom) samples as a function of frequency, recorded at 210 °C.

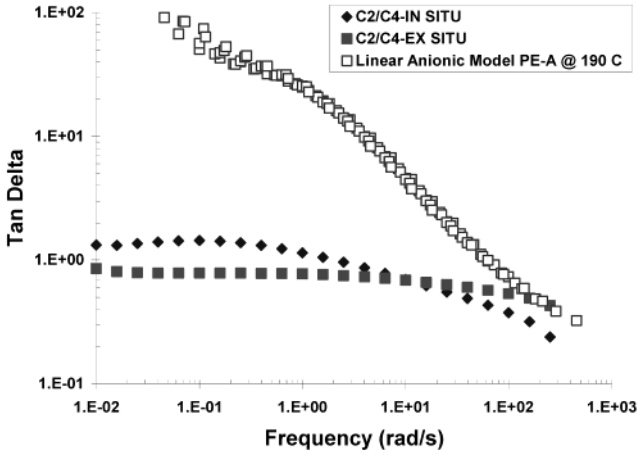

Figure 3. Plot of tan δ against frequency for ex-situ and in-situ samples relative to a model linear homo-polyethylene (synthesized by living anionic polymerization).

Analytical Crystaf Results. Figure 4 shows the Crystaf plots of the two polymer samples, showing the type and population of the crystalline components in the semicrystalline polymer. The ex-situ product displays three main fractions, while the in-situ sample has only two main fractions.

The area under the rectangular peak is proportional to the fraction of polymer that remained in solution at the end of the analysis. In the case of the ex-situ sample, there are two semicrystalline populations of more or less

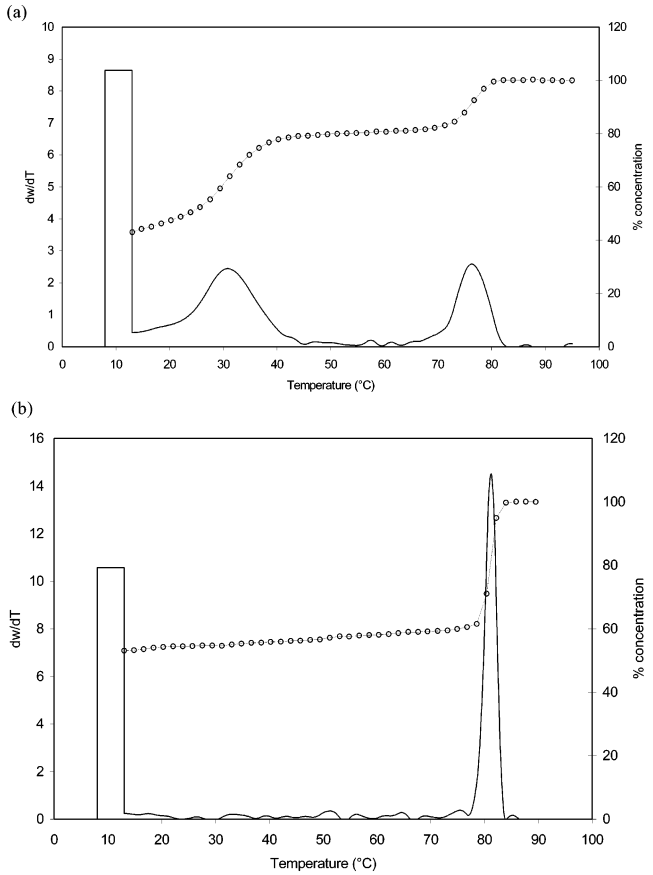

Figure 4. Crystaf profiles ex-situ (top) and in-situ (bottom) samples. The area of the rectangular section is proportional to the fraction of polymer soluble below the lowest crystallization temperature (15 °C for the in-situ sample and 30 °C for the ex-situ sample).

equal intensity centered at about 76 and 32 °C, besides the fraction that still remained in solution below 15 °C (lower fractionation temperatures were not attempted to avoid solvent freezing). The peak centered at 75 °C probably contains linear PE chains (Figure 1a) and some branch−block structures containing PE segments of high molecular weight (Figure 1c). The peak centered at 36 °C contains species of lower crystallinity, due to the formation of branch−block chains of the type shown in Figure 1c, where the molecular weight of the PE segments is not high enough. It can be speculated that the amorphous segments attached to the crystalline PE segments impair their ability to fit the crystal lattice, thus lowering their melting point. Finally, the amorphous fraction is mostly composed of linear and branched EB chains as represented in Figure 1b. It is possible that some EB chains containing very short PE segments will also be present in this fraction, though his has not been confirmed (such as by the C-13 NMR characterization of the Crystaf fractions).

In contrast, the in-situ product has only two major peaks. Keeping with the interpretation of the previous paragraph, it is clear that the in-situ product has a much smaller amount of branch−block polymer that the ex-situ polymer. The crystalline peak centered at about 80 °C is likely formed mainly of linear PE chains, while the amorphous peak is composed of linear or branched EB chains.

It is also interesting to notice that the two semicrystalline peaks of the ex-situ sample are broader than the

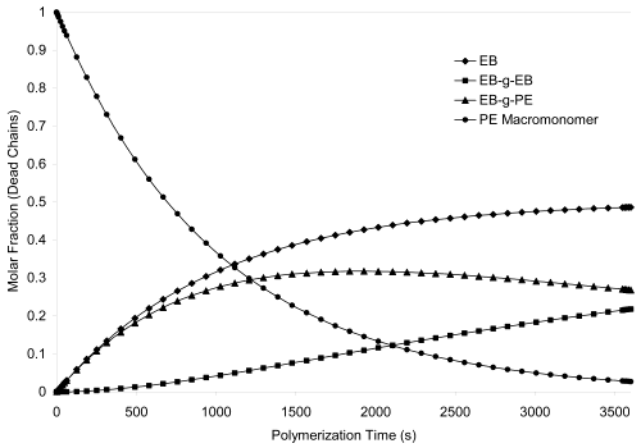

Figure 5. Concentration of dead polymer chains as a function of polymerization time for in-situ polymerization. Simulation parameters are $k_D Y = 1.0 \times 10^{-3}$ s^{-1}, $k_\beta/k_D = 2.0 \times 10^{-2}$ mol L^{-1}, and $m_0 = 0.02$ mol L^{-1}.

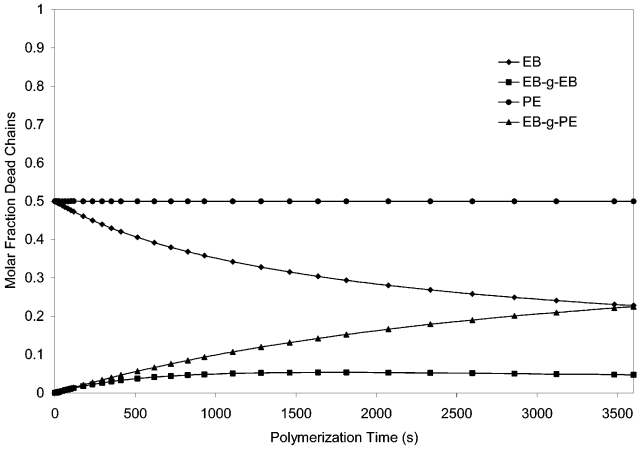

Figure 6. Concentration of dead polymer chains as a function of polymerization time for ex-situ polymerization. Simulation parameters are $k_{D1} Y = 1.0 \times 10^{-3}$ s^{-1}, $k_{D2} Y = 0$, $k_{\beta 1}/k_{D1} = k_{\beta 2}/k_{D2} = 2.0 \times 10^{-2}$ mol L^{-1}, and $\mu_1 = \mu_2 = 0.5$.

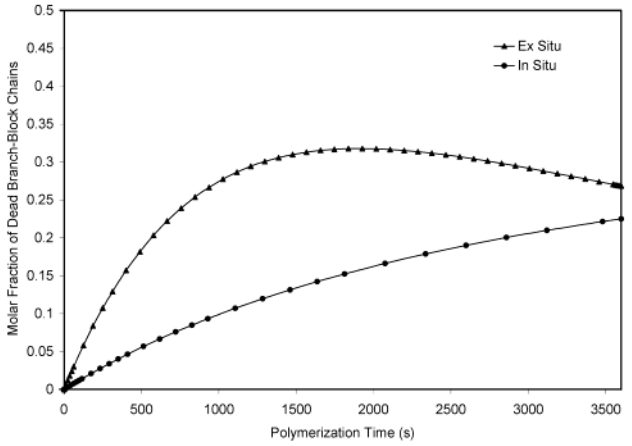

Figure 7. Fraction of branch−block chains as a function of polymerization time for several polymerization conditions. Simulation conditions are the same used for Figures 7 and 8.

80 °C peak of the in-situ sample, which is another indication that the ex-situ polymer is considerably more heterogeneous than the in-situ polymer.

Therefore, both microstructural and rheological characterizations seem to point out that the ex-situ sample contains a higher fraction of the desired cross-product EB-*g*-PE. These observations are also confirmed by mathematical modeling of this system, as described in the next section.

Simulations Results: Population Balances. The population balances presented in Table 2 were solved numerically in Matlab using an adjustable step size Runge−Kutta method. The resulting system of ODE is well behaved and very easy to integrate.

Figure 5 shows how the molar fractions of the different species of dead polymer change in the reactor as a function of polymerization time for the case of ex-situ polymerization. Model parameters were set arbitrarily to $k_D Y = 1.0 \times 10^{-3}$ s^{-1}, $k_\beta/k_D = 2.0 \times 10^{-2}$ mol L^{-1}, and $m_0 = 0.02$.

Notice that, since the concentration of macromonomer is at its maximum at the beginning of the polymerization, the polymer chains made initially are almost entirely heterogeneous (EB-*g*-PE). Supposing the polymerization can run long enough, the fraction of homogeneous branched chains will eventually increase, while the free macromonomer is consumed in the polymerization. Therefore, it is clear that this approach will always maximize the amount of branch−block chains formed in a semibatch polymerization.

Figure 6 shows similar results for the case the in-situ approach. Model parameters were set to the following arbitrary values: $k_{D1} Y = 1.0 \times 10^{-3}$ s^{-1}, $k_{D2} Y = 0$, $k_{\beta 1}/k_{D1} = k_{\beta 2}/k_{D2} = 2.0 \times 10^{-2}$ mol L^{-1}, and $\mu_1 = \mu_2 = 0.5$.

It is apparent that the formation of branch−block species in this case is completely different from the ex-situ case previously studied. Particularly, the rate of branch formation is much smaller at the beginning of the polymerization, since there is no macromonomer available for this reaction to take place at $t = 0$. If the catalyst deactivates in the reactor, this effect will be magnified even further.

These results agree well with the experimental evidence shown above. Since it is assumed that the block−branch chains are responsible for the appearance of the lower crystallinity shoulder in the Crystaf profile for the ex-situ run, it is illustrative to compare the rate of branch−block chain formation for several polymerization conditions (Figure 7). Notice how the formation of branch−block species at lower polymerization times is favored for the ex-situ approach. This is most likely the case of the samples analyzed by Crystaf in this study. Therefore, it can be proposed that the peak centered at 36 °C observed in the Crystaf profile of the ex-situ sample is due to these branch−block chains. The same is not observed for the in-situ synthesis because not enough of these species were formed during polymerization.

This is more clearly illustrated in Figure 8, where the microstructures of samples made in-situ and ex-situ are compared after 10 min of polymerization. Notice that these products have completely different microstructures and consequently will have distinct mechanical and rheological properties.

Simulation Results: Statistical Approach. The simulation results presented in the previous section help explain the enhanced formation of branch−block species during ex-situ polymerization, but the simplicity of the model does not allow the description of molecular weight details of the polymer formed during the polymerization.

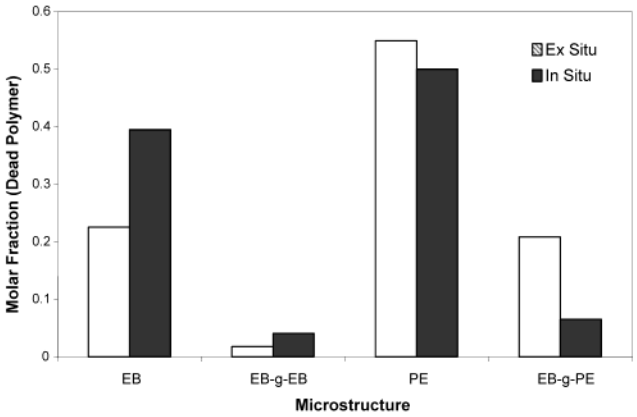

Figure 8. Molar fractions of the different chain structures present after 10 min of polymerization. Simulation conditions are the same used for Figures 7 and 8.

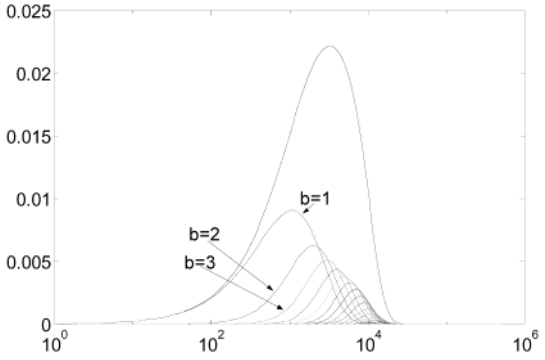

Figure 9. Population distribution of combs having a progression of branches.

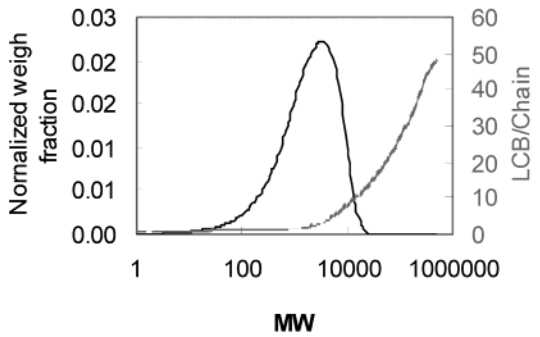

Figure 10. Molecular weight distribution and average number of LCB/chain EB-*g*-PE from model simulation.

This limitation can be overcome by using the statistical formulation described with eqs 1−6.

An example of model calculation is shown in Figure 9. For the cases presented in our earlier paper,[3] a significant fraction of molecules has one branch. The population of molecules with higher number of branches decreases with the number of branching. Species with higher number of branches are located at the high molecular weight end. Population distributions of all branched species can be averaged over the number of branching for all species. The averaged data are shown in Figure 10. The averaged number of branching increases with molecular weight, consistent with experimental observations on model PE-*g*-EB copolymers.[3]

Conclusion

Mixed-catalyst systems may well usher the next wave in polyolefin architecture design. Through detailed structural characterization and polymerization kinetic model simulation, we have shown that mixed-metallocene catalysts under different polymerization processes can yield architecturally different branch−block copolymers. The next challenge would be to establish the direct relationship between architectural details (e.g., the size and distribution of the PE blocks) and mechanical and flow properties of the polymers produced. Such an undertaking would require the application of more advanced fractionation and characterization tools. It will also benefit from more detailed kinetic data, the synthesis and study of model polymers, and mathematical models that could account for the distribution of various branch architectures. Even though many of these analytical and mathematical tools exist today, their application for mapping the complex structure−property patterns observed in the polymer systems resulting from the use of mixed catalysts is just beginning.

Appendix. Polymerization Pathways and Population Balance of Various Species

The kinetic scheme that represents the long-chain branching formation in a dual catalyst system is presented below. The model comprises the basic kinetic steps of olefin polymerization: initiation, propagation, termination, and the necessary steps for long-chain branch formation through macromonomer incorporation. The mechanism of LCB formation is copolymerization of vinyl-terminated macromolecules. Notice that catalyst 1 produces linear polymer chains only. It is also assumed that polymers ending with ethylene form vinyl chain ends through β-hydride elimination, and only these macromonomers can be incorporated to produce LCB.

initiation (catalyst 1 produce linear chains only)

$$C_1^* + M_1 \rightarrow P_1$$

$$C_1^* + M_2 \rightarrow Q_1$$

$$C_2^* + M_1 \rightarrow R_{1,0}$$

$$C_2^* + M_2 \rightarrow S_{1,0}$$

propagation

$$P_i + M_1 \xrightarrow{k_{p11}} P_{i+1} \quad k_{p11}$$

$$P_i + M_2 \xrightarrow{k_{p12}} Q_{i+1} \quad k_{p12}$$

$$Q_i + M_1 \xrightarrow{k_{p21}} P_{i+1} \quad k_{p21}$$

$$Q_i + M_2 \xrightarrow{k_{p22}} Q_{i+1} \quad k_{p22}$$

$$R_{i,b} + M_1 \xrightarrow{k_{p12}} R_{i+1,b} \quad k_{p12}$$

$$R_{i,b} + M_2 \xrightarrow{k_{p12}} S_{i+1,b} \quad k_{p12}$$

$$S_{i,b} + M_1 \xrightarrow{k_{p12}} R_{i+1,b} \quad k_{p12}$$

$$S_{i,b} + M_2 \xrightarrow{k_{p12}} S_{i+1,b} \quad k_{p12}$$

β-hydride elimination (polymer $P_{I,b}$ and $R_{I,b}$ are terminated with ethylene)

$$P_i \xrightarrow{k_{\beta 11}} P_i^{2-} + C_1^* \quad k_{\beta,11}$$

$$Q_i \xrightarrow{k_{\beta 11}} Q_i' + C_1^* \quad k_{\beta,11}$$

$$R_{i,b} \xrightarrow{k_{\beta 11}} R_{i,b}^{2-} + C_1^* \quad k_{\beta,11}$$

$$S_{i,b} \xrightarrow{k_{\beta 11}} S_{i,b}' + C_1^* \quad k_{\beta,11}$$

chain transfer (chain termination)

$$P_i + CTA \rightarrow P_i' + C_1^*$$

$$Q_i + CTA \rightarrow Q_i' + C_1^*$$

$$R_{i,b} + CTA \rightarrow R_{i,b}' + C_1^*$$

$$S_{i,b} + CTA \xrightarrow{k_t} S_{i,b}' + C_1^*$$

long-chain branching

$$R_{i,b} + P_m^{2-} \xrightarrow{k_{lcb11}} S_{i+m,b+1}$$

$$R_{i,b} + R_{m,n}^{2-} \xrightarrow{k_{lcb11}} S_{i+m,b+n+1}$$

$$S_{i,b} + R_{m,n}{}^{2-} \xrightarrow{k_{lcb11}} S_{i+m,b+n+1}$$

$$S_{i,b} + P_m^{2-} \xrightarrow{k_{lcb11}} S_{i+m,b+1}$$

catalyst deactivation

$$P_i \xrightarrow{k_d} P_i' + C_{1d}$$

$$Q_i \xrightarrow{k_d} Q_i' + C_{1d}$$

$$R_{i,b} \xrightarrow{k_d} R_{i,b}' + C_{1d}$$

$$S_{i,b} \xrightarrow{k_d} S_{i,b}' + C_{1d}$$

$$C_1^* \xrightarrow{k_d} C_{1d}$$

$$C_2^* \xrightarrow{k_d} C_{2d}$$

References and Notes

(1) (a) Kaminsky, W.; Kulper, K.; Niedoba, S. *Makromol. Chem. Macromol. Symp.* **1986**, *3*, 377. (b) Coates, G. W. *Chem. Rev.* **2000**, *100*, 1223−1252. (c) Alt, H. G.; Koppl, A. *Chem. Rev.* **2000**, *100*, 1205−1221. (d) Hlatky, G. G. *Chem. Rev.* **2000**, *100*, 1347−1376. (e) Resconi, L.; Cavallo, L.; Fait, A.; Piemontesi, F. *Chem. Rev.* **2000**, *100*, 1253−1345. (f) Ittel, S. D.; Johnson, L. K.; Brookhart, M. *Chem. Rev.* **2000**, *100*, 1169−1203. (g) Chen, E. Y.-X.; Marks, T. J. *Chem. Rev.* **2000**, *100*, 1391−1434. (h) de Souza, R. F.; Casagrande, O. L. *Macromol. Rapid Commun.* **2001**, *22*, 1293−1301. (i) Komon, Z. J. A.; Bazan, C. *Macromol. Rapid Commun.* **2001**, *22*, 467−478.

(2) Beigzadeh, D.; Soares, J. B. P.; Duever, T. A. *Macromol. Symp.* **2001**, *173*, 179−194.

(3) Markel, E. J.; Weng, W.; Peacock, A. J.; Dekmezian, A. H. *Macromolecules* **2000**, *33*, 8541−8548.

(4) Soares, J. B. P.; Beigzadeh, D.; Duever, T. A.; da Silva Filho, A. A. *Polym. React. Eng.* **2000**, *8*, 241−270.

(5) Soares, J. B. P.; Kim, J. D. *J. Polym. Sci., Part A: Polym. Chem.* **2000**, *38*, 1408−1416.

(6) Kim, J. D.; Soares, J. B. P. *J. Polym. Sci., Part A: Polym. Chem.* **2000**, *38*, 1417−1426.

(7) Kim, J. D.; Soares, J. B. P. *J. Polym. Sci., Part A: Polym. Chem.* **2000**, *38*, 1427−1432.

(8) Beigzadeh, D.; Soares, J. B. P.; Duever, T. A. *Macromol. Rapid Commun.* **1999**, *20*, 541−545.

(9) Kim J. D.; Soares, J. B. P.; Rempel, G. L. *J. Polym. Sci., Part A: Polym. Chem.* **1999**, *37*, 331−339.

(10) Soares, J. B. P.; Penlidis, A. In *Properties & Technology of Metallocene-Based Polyolefins;* Scheirs, J., Kamisnky, W., Eds.; John Wiley & Sons: Chichester, pp 237−267, in press.

(11) (a) Bishko, G.; McLeish, T. B. *Phys. Rev. Lett.* **1997**, *79*, 2352−2355. (b) Groves, D. J.; McLeish, T. C. B.; Ward, N. J.; Johnson, A. F. *Polymer* **1998**, *39*, 3877−3881. (c) Bick, D. K.; McLeish, T. C. B. *Phys. Rev. Lett.* **1996**, *76*, 2587−2590. (d) Orofino, T. A. *Polymer* **1961**, *2*, 305−314. (e) Schroff, R. N.; Mavridis, H. *Macromolecules* **1999**, *32*, 8454−8464. (f) Bonchev, D.; Markel, E. J.; Dekmezian, A. H. *J. Chem. Inf. Comput. Sci.* **2001**, *41*, 1274−1285. (g) Bonchev, D.; Markel, E. J.; Dekmezian, A. H. *Polymers* **2002**, *43*, 203−222. (h) Costeux, S.; Wood-Adams, P.; Beigzadeh, D. *Macromolecules* **2002**, *35*, 2514−2528.

(12) (a) Simon, L. C.; Soares, J. B. P. *Macromol. Theory Simul.* **2002**, *11*, 222−232. (b) Soares, J. B. P. *Macromol. Theory Simul.* **2002**, *11*, 184−198. (c) Hadjichristidis, N.; Xenidou, M.; Iatrou, H.; Pitsikalis, M.; Puolos, Y.; Avgeropoulos, A.; Sioula, S.; Parasveka, S.; Velis, G.; Lohse, D. J.; Schulz, D. N.; Fetters, L. J.; Wright, P. J.; Mendelson, R. A.; Garcia-Franco, C. A.; Sun, T.; Ruff, C. J. *Macromolecules* **2000**, *33*, 2424−2436.

(13) Smith, J. A.; Brzezinska, K. R.; Valenti, D. J.; Wagener, K. B. *Macromolecules* **2000**, *33*, 3781−3794.

(14) (a) Fetters, L. J.; Lohse, D. J.; Richter, D.; Witten, T. A.; Zirkel, A. *Macromolecules* **1994**, *27*, 4639.

(15) Nele, M.; Soares, J. B. P.; Dekemezian, A.; Pinto, J. C. *Macromol. Theory Simul.*, submitted.

(16) (a) Stejskal, J.; Horská, J.; Kratochvil, P. *Macromolecules* **1984**, *17*, 920−926. (b) Stejskal, J.; Kratochvil, P.; Jenkins, A. D. *Macromolecules* **1987**, *20*, 181−185.

(17) Gu, L.; Zhu, S.; Hrymak, A. N. *J. Polym. Sci., Part B: Polym. Phys.* **1998**, *36*, 705−714.

(18) (a) Zhu, S. *Macromolecules* **1998**, *31*, 7519−7527. (b) Zhu, S.; Li, D.; Zhou, W.; Crowe, C. M. *J. Polym. Sci., Polym. Phys.* **1994**, *32*, 929−935.

(19) Sun, T.; Brant, P.; Chance, R. R.; Graessley, W. W. *Macromolecules* **2001**, *34*, 6812−6820.

(20) Monrabal, B. *J. Appl. Polym. Sci.* **1994**, *52*, 491.

(21) Garcia-Franco, C. A.; Srinivas, S.; Lohse, D. J.; Brant, P. *Macromolecules* **2001**, *34*, 3115−3117.

(22) Kokko, E.; Pietikainen, P.; Koivunen, J.; Seppala, J. V. *J. Polym. Sci., Part A: Polym. Chem.* **2001**, *39*, 3805−3817.

(23) Wood-Adams, P. M.; Dealy, J. M.; deGroot, A. W.; Redwine, D. D. *Macromolecules* **2000**, *33*, 7489−7499.

MA0209343